Degradation of tetracycline using photocatalytic membrane reactor with nanocomposite Ag doped clinoptilolite zeolite photocatalyst

Milad Hallajiqomi, Mohsen Mehdipourghazi*, Farshad Varaminian

Faculty of Chemical, Petroleum and Gas Engineering, Semnan University, 35131-19111, Semnan, Iran, email: sos313@gmail.com (M. Hallajiqomi), Tel. +98 2333383922, Fax +98 2333654284, email: mohsenmehdipour@semnan.ac.ir (M. Mehdipourghazi), fvaraminian@semnan.ac.ir (F. Varaminian)

ABSTRACT

A photocatalytic membrane reactor was tested in the Degradation of Tetracycline from water using photocatalyst clinoptilolite zeolite-silver. Photocatalyst clinoptilolite zeolite-silver synthesized using a microwave energy technique. The prepared photocatalyst was authenticated by XRD, FESEM, BET and DRS analysis methods. In this study, the influence of AgO in photocatalytic membrane reactor has been investigated for Tetracycline treatment. The experiments were done to appraise the influence of various empirical factors i.e., pH, photocatalyst dosage and irradiation time on the degradation efficiency. The results showed that optimum conditions for tetracycline degradation were found to be at pH of 9, photocatalyst dosage of 0.8 g/L and irradiation time of 120 min. The point of zero charge (pzc) of photocatalyst clinoptilolite zeolite-silver, the point when the surface charge density is zero, was identified be of 8. The photocatalytic treatment achieved between 50% and 94% of Tetracycline degradation and up to 98% chemical oxygen demand (COD) removal.

Keywords: Membrane photocatalytic reactor; Tetracycline; Degradation; Microwave irradiation; Silver-modified clinoptilolite

1. Introduction

Antibiotics have a broad application in medicine for animals and also in their feed stuff as an additive. They improve growth and restrain the spread of the disease and also improve the efficiency [1]. The presence of pharmaceutical ingredients in aqueous environment (pharmaceutical residues, from sewage effluents, hospital waste, animal excrements, and improper disposal of unused drugs) has raised increasing concerns in recent years [2]. It seems probable that most urban wastewater is contaminated with medicinal compounds which affects the water quality and drinking water supplies and may constitute a potential risk for the ecosystems and the human and animal welfare in the long term [3–5]. TC which stands for Tetracycline have been highly applied in medicine for humans and animals in order to prevent bacterial infections and to treat them and they are used more compared to other antibiotics. There are some reports that TCs have toxic impacts on vegetarian life, bacteria from wastewater sludge and no target organisms [6]. Fig. 1 shows the most conventional TCs which are chlortetracycline (CTC), oxtetracycline (OTC), and doxycycline (DC) [7].

Due to the foretold reasons, the act of eliminating or reducing the pharmaceutical pollutants is a necessary topic for research. There are outstanding endeavors to develop a way to purify and demolish the bio-recalcitrant organic contaminants properly [8]. It is not possible to remove antibiotic residues in an effective manner by using customary biological methods because their nature is antibacterial. Various researches have revealed the fact that at the time of wastewater treatment, there are low amounts of biodegradation in case of certain antibiotics [9,10]. In recent two decades, advanced oxidation processes (AOPs)

*Corresponding author.
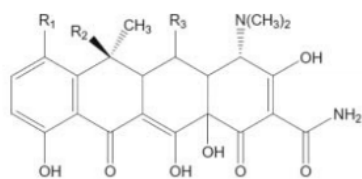
Compound	R_1	R_2	R_3
Tetracycline	H	OH	H
Oxytetracycline	H	OH	OH
Chlortetracycline	Cl	OH	H
Doxycycline	H	H	OH

Fig. 1. Chemical structures of the four tetracyclines.

such as photo-Fenton, photo-oxidation, photo-reduction and photocatalytic technologies have been widely used for the removal of different organic pollutants from water [11,12]. Although common homogeneous Fenton systems offer a cost-effective source of hydroxyl radicals, they have following drawbacks which can limit its industrial applications: (i) the tight working pH range, (ii) the need for recovering the precipitated catalyst after treatment and (iii) deactivation by some ion-complexing agents like phosphate anions. The resulting sludge may also contain organic substances as well as heavy metals and must be treated further, thus increasing the overall costs. Heterogeneous photocatalysis has proven to be the most suitable for the widespread environmental applications due to its chemical inertness, strong oxidizing power, cost effectiveness and long-term stability [13,14].

In the previous researches, there are various methods that have been proposed in order to remove these pharmaceutical components from water or wastewater flows. Some of these approaches are ultrasound and ozonation. Other methods like Fenton or photo-Fenton systems can also be found among the proposed techniques in order to purify the water. The process of adsorbing the pollutants with the activated carbon is among them and also the reverse osmosis is an also reliable approach. In the previous researches it has been proposed to utilize the method of photolysis with hydrogen peroxide (UV/H_2O_2). AOP stands for advanced oxidation process. The AOPs that has been developed in recent times like photocatalytic process are considered to be one of the best methods in case of efficiency for aqueous environment treatment. These photocatalytic processes utilize the hydroxyl radicals (OH) that are produced because they are able to react with a wide range of pollutants in water and wastewater flows. This results in their disintegration into CO_2 and H_2O [15–17].

MF and UF is being applied to a great extent in the hybrid systems along with photocatalysis to remove organic pollutants which include pharmaceuticals, nitrophenol, humic, and dyes [18,19]. Nonetheless, the impact of removing virus in the PMR has not been fully researched. Investigations have been done to analyze the impact of various functioning parameters on PMRs like the pattern of water feeding, hydraulic retention time and permeation mode with the goal of achieving a discharge with good quality [20–22].

Reactors using photocatalytic membranes can be categorized into two major types: (I) the type that has catalyst suspended in feed solution and (II) the type that has catalyst supported in/on the membrane. In the type that has photocatalyst in suspension; a membrane filtration may be applied as one step for the catalyst particles to be totally recovered from the solution [23,24].

During the years, natural and synthetic zeolite materials have proven to have outstanding ionic, adsorption and catalytic exchange properties [5–8,25]. Ion exchange appears to be an interesting approach compared to the various methods for removing heavy metal. This method is efficient and it remains that way when the concentration of contaminants are very low and the time that the cost is low and plentiful ion-exchangers are applied, it is not cost effective. Zeolites (particularly the natural zeolites) are proper ion-exchangers and because they have significant characteristics, they are frequently being used in various industrial processes [26–28].

In this research the results gained in the time of photocatalysis accomplished in the PMR applying α-alumina membrane are explained. The presence of photocatalyst clinoptilolite zeolite-silver (CP/Ag) in a feed on the process performance was investigated. In this work the photocatalyst CP/Ag synthesis was used by applying a microwave energy technique. The particles of zeolite were used to obtain clinoptilolite/Ag as a heterogeneous catalyst for the degradation of Tetracycline (TC) in an aqueous solution under visible light via a simple method. Clinoptilolite zeolite (CP) was the adsorbent of choice due to its good adsorption property and availability at an affordable cost. The research investigated the impacts that the initial Tetracycline concentration, photocatalyst amount, and pH have on the efficiency of the degradation. The properties of the as-prepared samples were determined by XRD which stands for X-ray diffraction, FE-ESM which stands for field emission scanning electron microscope (Mira 3-XMU, TESCAN Company), BET which stands for Brunner-Emmet-Teller method (belsorpmimiII japan), UV–Vis spectrophotometer (Avantes, Avaspec-2048-TEC) and diffuse reflection spectroscopy (DRS).

2. Experimental

2.1. Materials and method

Materials used in this work were silver nitrate ($AgNO_3$), sodium hydroxides (NaOH), acetone (($CH_3)_2CO$) and sulfuric acid (H_2SO_4) and all were obtained from Merck Company. Tetracycline tablets (which are presented in Table 1) were supplied from SinaDarou Laboratories. In the research deionized water was applied and all the other materials were applied without changing their initial condition.

Table 1
Chemical structure and characteristics of Tetracycline antibiotics[1]
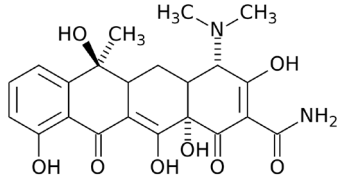
Chemical structure	
Molecular formula	$C_{22}H_{24}O_8N_2 \cdot HCl$
M_w (g/mol)	480.9
λ_{max} (nm)	360
Solubility in water (mol/L)	0.041
pK_{a1}	3.2 ± 0.3
pK_{a2}	7.78 ± 0.05
pK_{a3}	9.6 ± 0.3
Trade name	TC

Fig. 2. Schematic diagram of the laboratory-scale photocatalytic membrane reactor used in the experiments and top view of reactor.

2.2. Synthesis of photocatalyst clinoptilolite zeolite-silver

Silver (Ag) modification of clinoptilolite (CP) zeolite was obtained by the ion exchange process with shaking 20 g of clinoptilolite zeolite in 500 mL of 3% (w/v) $AgNO_3$ which was kept under reflux at 60°C for 24 h with magnetic stirring. In order to inhibit the precipitation of the silver ions, the solution's pH was set to 5. The solution was shaken for 12 h without the presence of light (due to the light sensitivity of silver) with the goal of obtaining the maximum exchange of silver onto the zeolites. The silver modified clinoptilolite zeolite (CP/Ag) was separated from the solution by filtration. It was then washed with deionized water and dried at 100°C for 24 h. It then calcined at 500°C for 3 h. After that the samples were transferred to small vials and stored in the dark.

2.3. Photocatalytic degradation experiments

A photocatalytic reactor with two lamps (Philips, 120 W) was used as the visible irradiation source to degrade the TC. With the purpose of producing the TC solution, the contents of an effective material was dissolved in water and shaken for 45 min; then it was filtered in a 1000 mL volumetric flask and diluted with water. The photoreactor was filled with 300 ml of 25 mg/L pollutant and 0.5 g/L of photocatalyst at an irradiation time of 120 min. The whole reactor was cooled with a water cooled jacket on its outside. The temperature was maintained at 26°C. With the purpose of allowing the TC molecules to adsorb on the CP/Ag surface, before photodecomposition the solution which contained a fixed amount of the photocatalyst was blended for 30 min in the absence of any light. In order to set the adsorption/desorption equilibrium of the pollutant on a heterogeneous catalysts surface, the reactor was kept under dark conditions for 45 min. An aliquot suspension was withdrawn and centrifuged at 6000 rpm to remove the solid particles. The UV–Vis absorption spectra of the TC solution which was scanned and showed an optimum band centered at 360 nm. It can be utilized as the absorbance wavelength for the formation of the TC standard curve based on the Lam-

bert–Beer law. The standard curve can be utilized in order to quantify the concentrations of different TC samples.
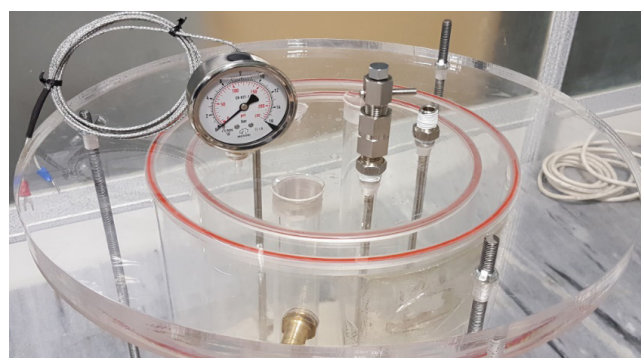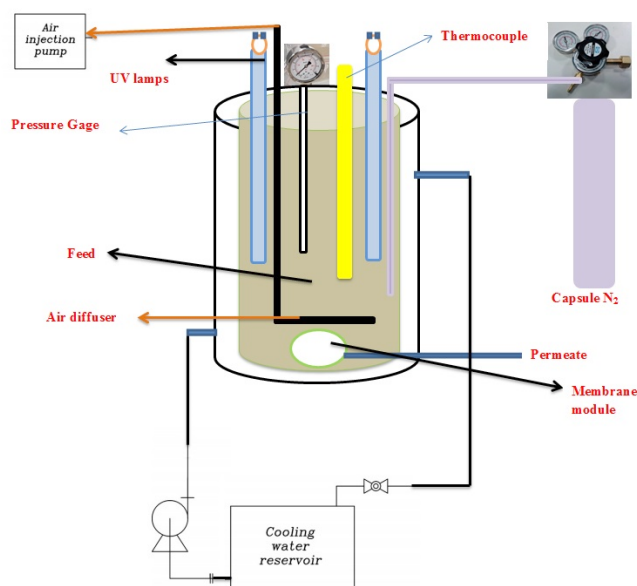
The degree of degradation was calculated by the following formula which is based on the absorbance of the solution (at λ_{max} = 360 nm) before and after irradiation.

$$TC \; degradation \; \% = \left[\frac{(C_o - C_t)}{C_o} \right] \times 100 = \left[\frac{(A_o - A_t)}{A_O} \right] \times 100 \quad (1)$$

where C_o and C_t stand for the initial and final concentration of TC at time t and A_o and A_t represent the initial and final absorbance of the samples. The absorbance values were used to calculate the percentage of degradation.

After a defined time of irradiation, the samples of feed solution were filtered through a 50–100 nm membrane filter and analyzed.

2.4. Model virus removal in PMR

Fig. 2 shows that the experiments were done in the reactor which has the volume of 10.5 L (m) and was fitted, with

two lamps (Philips, 120W). The disc α- alumina membrane (provided by Danesh Pajhohan Sanate Nano Company of Iran, pore size of 50–100 nm, membrane area of 0.002826 m^2, radius 3 cm, Thickness 5 mm and flux of pure water at P = 2,4 bar respectively 50.4, 116.2 L/h·m²) was gathered in the bigger part of the reactor. By measuring the volume of the permeated current that passes through the membrane in a specific time, its flux is estimated. In order to approve the reproducibility of the results, the experiments were repeated at least twice.

SEM or scanning electron microscope was utilized in order to determine the characteristics of the surface morphology and cross section. The images obtained from the SEM were presented in supporting materials (Fig. 3). NaOH and H_2SO_4 solutions were used to chemically clean the brand new membranes before the experiments and it is done in accordance with the protocol that was proposed by the manufacturer.

3. Results and discussion

3.1. Characterization of products by XRD

Fig. 4 shows the XRD pattern of CP zeolite collected at the bottom of the autoclave. The XRD data of natural used clinoptilolite and those of reference [29,30] are shown in Table 2. XRD analyses were performed for each mixture and peak intensity summation was calculated for 3 characteristic peaks (2θ = 9.84, 11.17, 22.35) of clinoptilolite. One of the products, BC 4, which was synthesized in this study and has the highest intensity summation, was selected as 100% clinoptilolite. The comparative XRD spectra of CP zeolite synthesize and Ag-doped zeolite (CP/Ag) are presented in Fig. 4. The thermal treatment of Ag-doped zeolite caused the intensities of reflection observed at about 8.7°, 10.45°, and 21.95° relating to the quantity of clinoptilolite to reduce [12,31]. The presence of low amount of silver in zeolite showed no important difference in the patterns of
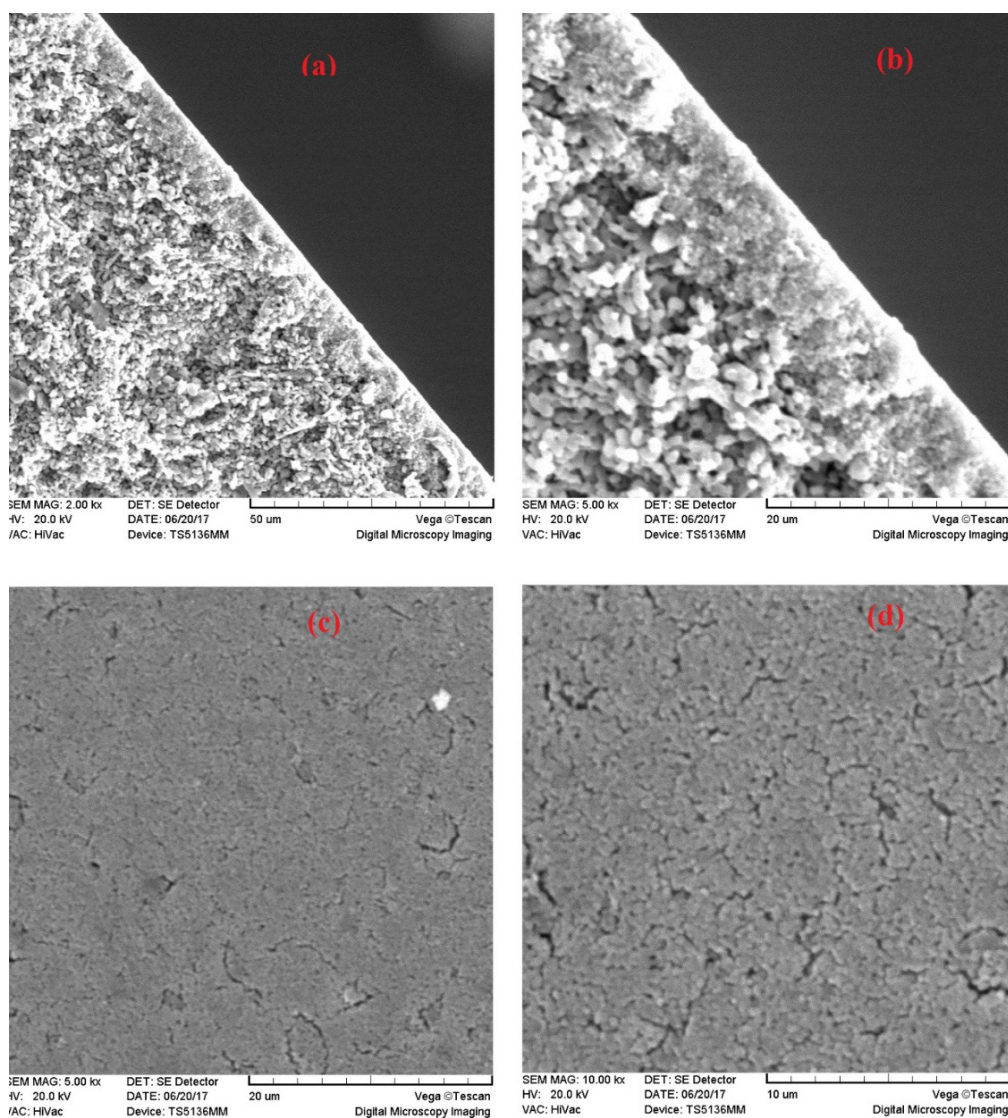
Fig. 3. SEM images of: (a), (b) cross section and (c), (d) the surface morphology α- alumina membrane.
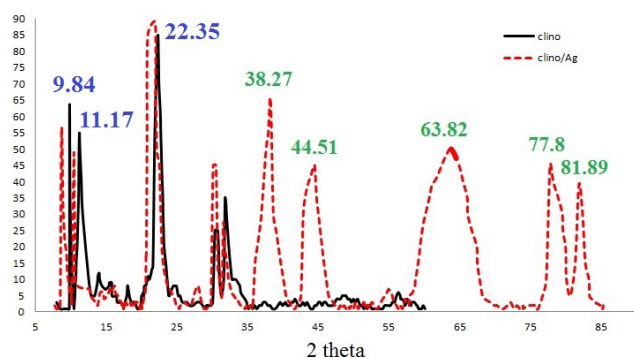
Fig. 4: X-ray Diffraction Data of Synthetic Clinoptilolite zeolite and Ag-doped Clinoptilolite zeolite.

Table 2
XRD data of natural clinoptilolite and reference [36]

d_{exp}	d_{ref}	RE%	I_{exp}	I_{ref}
8.93	8.96	0.31	13.3	100.0
7.92	7.91	0.13	20.0	40.1
6.78	6.77	0.12	14.3	15.8
5.79	5.78	0.15	9.0	15.8
5.23	5.24	0.19	15.4	17.6
5.12	5.11	0.22	6.7	3.2
5.07	5.06	0.20	19.8	17.2
3.97	3.98	0.15	100.0	55.4
3.95	3.96	0.05	18.0	20.5
3.55	3.56	0.14	15.5	16.8
3.42	3.42	0.05	69.2	36.7
3.31	3.32	0.15	4.3	11.3
3.17	3.17	0.03	32.4	31.1
2.97	2.97	0.10	42.8	30.7
2.97	2.96	0.10	9.6	20.4
2.78	2.78	0.07	25.7	26.7
2.78	2.77	0.29	47.5	26.7
2.73	2.74	0.22	12.5	5.5
2.72	2.73	0.33	2.7	11.1
2.53	2.53	0.20	1.8	2.2
2.45	2.44	0.37	19.6	7.1
2.13	2.13	0.19	1.8	2.4
2.08	2.09	0.24	3.2	3.9
1.92	1.91	0.31	1.5	1.2

diffraction. Nevertheless, traces of $AgAlO_2$ (26.19°; 31.58°) were identified.

The crystalline size is determined by applying Debye-Scherrer formula [32,33]:

$$D = k\,\lambda/\beta\,\cos\theta$$

where D is the crystalline size, β is the full width half maximum (FWHM) of the 2θ peak, K is the shape of particle factors (it equals to 0.78), θ and λ are the incident of angle and wavelength of the X-rays, respectively. The average crystalline size of CP/Ag NPs associated with all the diffraction peaks was estimated about 24.6 nm, respectively.

3.2 Morphology of products by FE-SEM

Fig. 5 presents the FE-SEM images of clinoptilolite zeolite that is thermally treated and Ag-doped. Fig. 5 shows the considerable changes of the morphology of Ag-doped zeolite in correlation with the synthesized clinoptilolite zeolite. Some small particles which were agglomerated on the zeolitic material were noticed [34]. The metallic Ag particles were noticed to distribute homogenously on the zeolite clusters' surface. The agglomeration of more silver particles on the Ag-zeolite composites' surface may have caused the composite cluster size to become larger. Moreover, another reason for the cluster size of the CP/Ag composites getting larger could be the nucleation and growth of the metallic Ag inside the zeolite internal pores [35].

3.3. BET surface area analysis

The surface area (S_{BET}) of the samples was determined from the N_2 adsorption-desorption isotherms using the Brunner-Emmet-Teller method. The surface area of BET for the prepared photocatalysts is shown in Table 3. In a different research, the surface area and average pore diameter of different percentages of AgO on the zeolite were observed. The surface texture properties of the raw clinoptilolite (CP), Ag supported clinoptilolite (CP/Ag) samples were
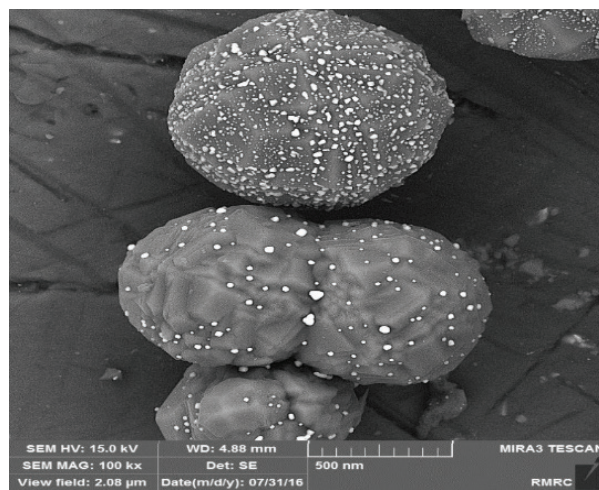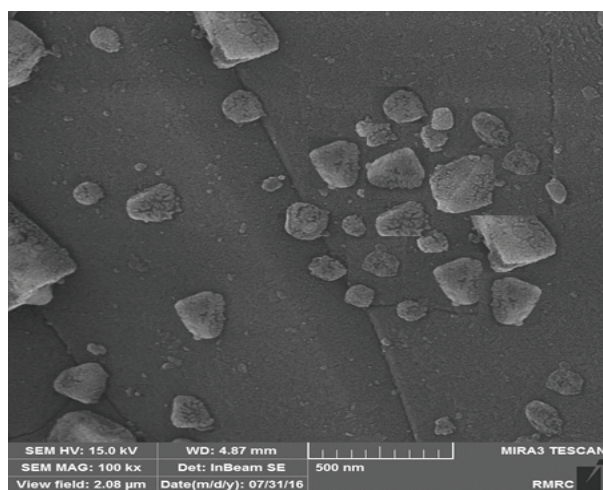
Fig. 5. FE-SEM images of Ag-doped Synthetic Clinoptilolite zeolite.

Table 3
BET surface area results for various prepared samples

Sample	S_{BET} (m^2/g)	V_p (cm^3/g)	d_p (nm)	Constant C
AgO	23.81	2.42	28	32.8
(CP)	235.93	5.95	26.74	1011.8
CP/Ag	167.24	4.05	45.88	253.85
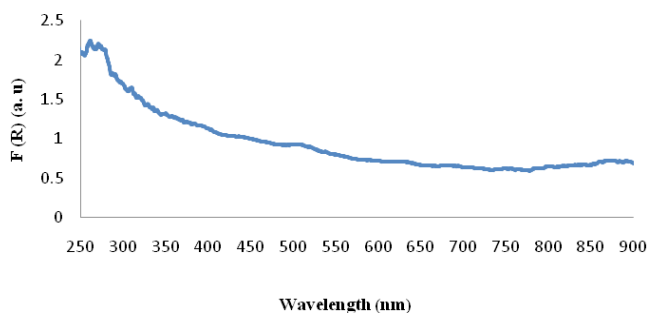
Fig. 6. UV–Vis diffuse reflectance spectra of commercial Ag-doped Clinoptilolite zeolite sample.

determined by N$_2$ adsorption and the obtained results are summarized in Table 3. As shown, because of the possible blocking of some zeolite pores by Ag, Ag semiconductor by clinoptilolite reduces the surface area and also the total pore volume. The formation of Ag in the zeolite channels and surface causes the solid particle size to go higher and the surface area and pore volume to become smaller [36,37].

3.4. DRS studies

The UV–vis diffuse reflectance spectroscopy (DRS) was applied in order to investigate the optical characteristics of catalyst and is presented in Fig. 6. Clearly, the CP/Ag catalyst was able to absorb both the UV and visible light well. It can be seen that the CP/Ag sample, showed absorbance in the visible range which suggested its potential to be activated by visible light. Using UV-vis spectra to determine the band gap was an alternative approach to investigate the modification of the electronic property of the synthesized species. The energy band structure was a key factor affecting the photocatalytic activity of catalysts [38]. By using the definitions in physics, if there is an energy range in the solid that at that range none of the electrons can have an existing state, that range can be called a band gap. For example in semi-conductors, if the energy difference that exists from the valence's top to the conduction band's bottom be measured, this amount can be related to the band gap. This energy actually is the exact amount of energy that is sufficient in order to take a valence electron bound higher in an atom and therefore the so-called electron will be a conduction electron after that. This electron can then transfer inside the crystal lattice very freely. Thus these transferring electrons can be the charge carriers which mean they can transfer electricity. But in some situations the so-called electrons are not able to transfer. These situations consist of two conditions. One is that the valence band is totally full and the other is that the conduction band be totally empty.

On the other hand, in the situation that there are electrons which are able to move from the valence to the conduction band, electric current can occur. Thus, the band gap is the main parameter for determining the electrical conductivity of a solid [38–41].

Tauc's equation estimates the band gap of the composite by applying the absorption data [39]:

$$\alpha = \alpha_0 (h\nu - E_g)^n / h\nu$$

α represents the coefficient of absorption, h and α_0 are the constants, $h\nu$ represents the energy of the photon, E_g pertains the material's optical band gap and n is dependent on the electronic transition type and its value is between 0.5 and 3. Extrapolation of the linear portion of the plots of $(\alpha h\nu)$ 0.5 against $h\nu$ to the energy axis was done to recognize the sample's energy gap (Eg).

The following formula can determine the valence band (VB) and conduction band (CB) potentials of the semiconductor at the point of zero charge:

$$E_{VB} = X - E_c + 0.5\, E_g$$

E_{VB} or E_{CB} represent the VB or CB edge potentials of semiconductor, X pertains the absolute electronegativity of its constituent atoms, E_c stands for the free electrons' energy on the hydrogen scale (ca. 4.5 eV), and E_g represents the band gap of semiconductor. The CB position can be calculated by $E_{CB} = E_{VB} - E_g$ [39]. Since zeolites generally do not absorb any light in UV–vis regions, they are one of the most suitable supports for photocatalysis. The results revealed a clear trend in decreasing the band gap of commercial AgO to 2.47 eV for Ag supported on CP. This suggested that the particle size of AgO supported on zeolite was larger than that of commercial AgO which was used in the present study (quantum size effect) [40,41]. Furthermore, zeolite delocalizes the band-gap excited electrons of Ag and therefore minimizes the electron/hole recombination.

3.5. Photodegradation mechanism

The proposed mechanism of photocatalytic performance, photoexcitation, and charge transfer in CP/AgO under visible light irradiation is shown in Fig. 7. Under visible light irradiation AgO shows no photoelectronic response due to the wide band gap (2.47 eV), while both Ag and AgO nanoparticles were excited and produced h$^+$ and e$^-$ as mentioned in formula:

$$Ag^+ + h\nu \rightarrow Ag^{2+} + e^- \tag{2}$$

$$2AgO + h\nu \rightarrow 2Ag + O_2 \tag{3}$$

We proposed that trapped electrons could be transferred to oxygen on the nanocomposite surface and produce superoxide radical, or could further react with AgO and reduced it to Ag.

$$O_2 + e^- \rightarrow O^- \tag{4}$$

$$2AgO + e^- \rightarrow 2Ag + O_2 \tag{5}$$
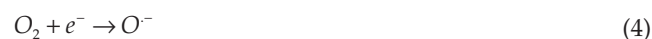
The generated anion superoxide and holes in AgO react with adsorbed H_2O on the surface of nanocomposite and produce active $^{\bullet}OH$ species. It is assumed that the generated hydrogen peroxide converts to $^{\bullet}OH$ species with three possible reactions.

$$O_2 + H_2O \rightarrow HO_2 + OH^- \tag{6}$$

$$H_2O + h^+ \rightarrow \cdot OH + H^+ \tag{7}$$

$$O_2^- HO_2 + H^+ \rightarrow H_2O_2 + O_2 \tag{8}$$

$$H_2O_2 + e^- \rightarrow \cdot OH + OH^- \tag{9}$$

$$H_2O_2 + h\nu \rightarrow \cdot OH \tag{10}$$

$$H_2O_2 + O_2^- \rightarrow \ OH + OH^- + O_2 \tag{11}$$
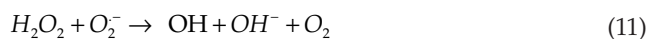
TC can be oxidized by the trapped holes on AgO nanoparticles or free reactive $^{\bullet}OH$ species in the solution and decomposed to carbon dioxide, water and other inorganic components.

$$TC + \cdot OH(h^+) \rightarrow H_2O + CO_2 + degradation \_ products \tag{12}$$
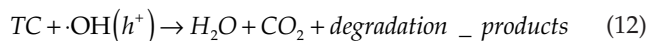
Based on Fig. 8 it can be concluded that the decrease in absorption at 360 nm band is related to a low degree absorption in the visible region which is because of the formation of 4a, 12a-anhydro-4-oxo-4-dedimethylaminote-tracycline [42]: Photodegradation of TC happens in an easy way and a high number of degradation compounds has been transformed by it. In most photolysis processes, side-chain degradation by desulfurization, deamination and dealkylation is a common phenomenon. Photo deamination happens after the TC exposure to UV irradiation. Based on the 22 atoms of tetracycline, removing volatile dimethylamine requires the loss of just 2 carbon atoms [42].

3.6. Effect of pH on permeation flux and the degradation efficiency

The aqueous solution's pH is a major factor to control the process of degradation. With the aim to investigate the impact that pH has on the efficiency of the TC degradation, 50 mL of TC solution which had the initial concentration of 25 ppm in distilled water was treated with 500 mg of CP/Ag nanophotocatalyst and 500 mg of CP at different pH values. The results are summarized in Table 4. It was concluded that the degradation of TC by applying CP/Ag nanophotocatalyst is highly dependent to pH. In aqueous media, the surface of photocatalyst is positively charged in acidic solution and negatively in alkaline solution and TC is a cationic/basic. As a result, it is not surprising that the adsorption of TC of the solution is high. The number of the molecules on the surface of photocatalyst in alkaline solutions\increases, causing the increase in degradation efficiency of TC [43]. On the other hand, higher pH values
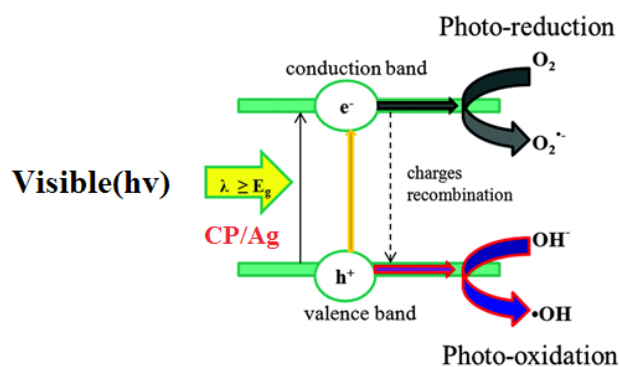
Fig. 7. Schematic view of proposed charge transfer mechanism of CP/Ag photocatalyst under visible light radiation.

Table 4
Effect of pH in TC degradation: photocatalyst dosage, 0.5 g/l; irradiation time, 2 h at 26°C

Type of photocatalyst	pH	Initial conc. (ppm)	Degradation efficiency (%)
	5	25	38
	6	25	56
CP/Ag	7	25	79
	8	25	86
	9	25	94
CP	5	25	4
	6	25	11
	7	25	17
	8	25	21
	9	25	26
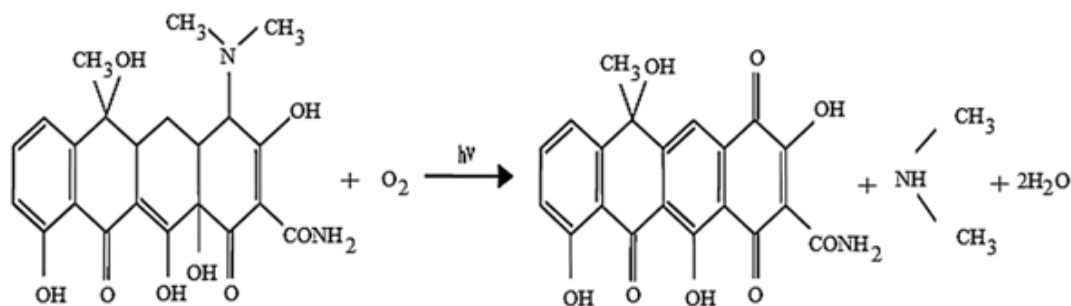
Fig. 8. Photodegradation of TC into 4a, 12a-anhydro-4-oxo-4-dedimethylaminotetracycline.
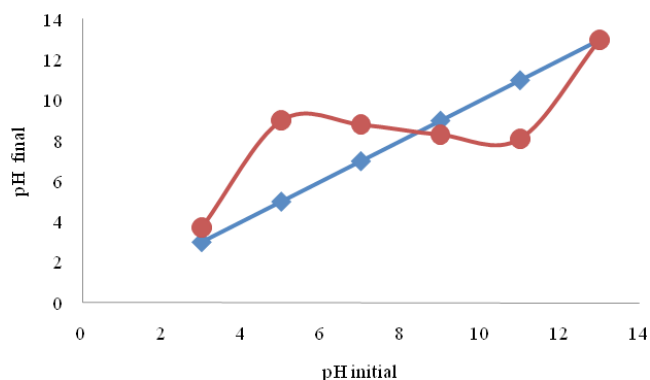
Fig. 9. pH$_{PZC}$of Photocatalyst Clinoptilolite Zeolite-Silver.

can provide higher concentration of hydroxide ions to react with the holes to form hydroxyl radicals. The deactivation of •OH is also more important when pH of the solution is high.

The point of zero charge (pzc) of photocatalyst clinoptilolite zeolite-silver, the point in which the density of the charge in the surface becomes null, was identified to be 8 and is shown in Fig. 9. This value is corresponded to the pH at which the straight line (pH$_{initial}$ = pH$_{final}$) crossed the sigmoid curve passing through the experimental points [44]. The characteristics of the electric charge for the catalyst and also for the substrate had a significant impact on the process of adsorption. At pH < pH$_{pzc}$the catalyst's surface was positively charged, at pH > pH$_{pzc}$ it was negatively charged, and at pH = pH$_{pzc}'$ it stayed neutral. This reaction highly affected the adsorption–desorption properties of the surface of the catalyst and it also had effect on the alterations in the structure of the pollutant at different pH values. In addition, the pKa$_1$, pKa$_2$ and pKa$_3$ values of the TC molecule are 3.3, 7.68, and 9.7, respectively, which are related to equilibriums (TCH$_3^+$ → TCH$_2$, TCH$_2$ → TCH$^-$, and TCH$^-$ → TC$_2^-$). The adsorption mode and the concentration of OH were two key factors influencing the photocatalytic degradation efficiencies of TC at different pH values [8,45]. The pH$_{PZC}$ of the synthesized catalyst was found to be about 8. The adsorption of TC on the catalyst might be inhibited by the enhanced electrostatic repulsion between H$_3$TC$^+$ and the positively charged catalyst at a pH of 5 as well as between HTC$^-$/TC$_2^-$ and a negatively charged catalyst at a pH of 9 and 11, respectively. Also, in a pH = 9, the TCH$^-$ and TC$_2^-$ species were dominant and the surface of the nano composite particles had a positive charge. Thus, the TC molecule seemed to be attracted to the positively charged CP/Ag surface.

Accordion to Fig. 10, although the observed increase in the experiment that was done at pH 13, at all of the pH values that were researched, the normalized permeability flux stayed constant. This behavior showed that the fouling that was seen in the alkaline medium was just a physical process.

3.7. Effect of photocatalyst dosage on permeation flux and the degradation efficiency

Catalyst loading is an important factor which cans significantly influence the photocatalytic degradation rate
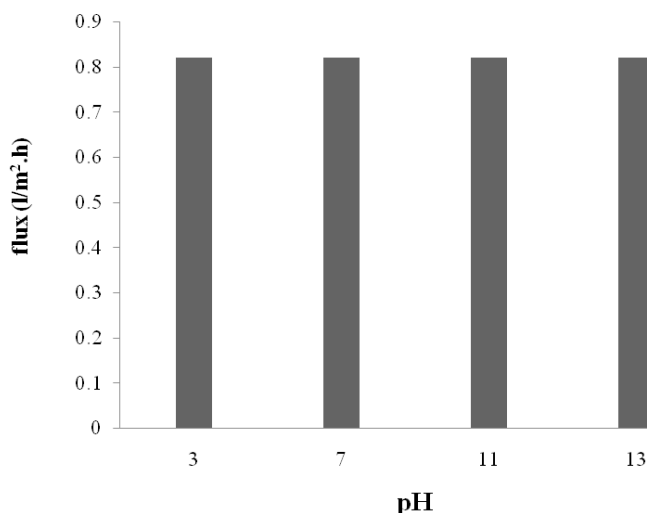
Fig. 10. The effect of pH on permeation flux.
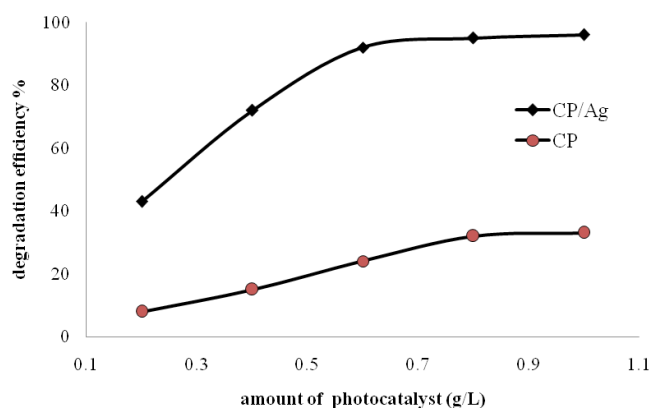
Fig. 11. The effect of photocatalyst dosage on degradation efficiency of TC: pH, 8; initial concentration, 25 mg/L; irradiation time, 2 h at 26°C.

[46]. The effect of photocatalyst clinoptilolite zeolite-silver and clinoptilolite zeolite on the pollutant degradation was analyzed when their concentration was between 0.2–1 g/L through the constant initial TC concentration of 25. As shown in Fig. 11, increasing the concentration of the catalyst enhanced the efficiency of degradation. The increase in surface area or sites that are activated caused it. Nevertheless, its worth of attention that adding more amounts of catalyst can change the process of degradation in a way that it is less efficient. The increase in scattering and turbidity effects was actually related to that because it inhibits the penetration of light into all particles' surfaces [46–49]. The increase in the catalyst amount actually increases the number of active sites on the surface of the photocatalyst, thus causing an increase in the number of produced •OH radicals [50]. But, due to an increase in turbidity of the suspension because of the high dose of the catalyst, penetration of photons decreases which in turn decreases the photoactivated volume of the suspended catalyst [50]. Thus, it can be concluded that higher dose of the catalyst may not be useful due to negative effects of aggregation and light scattering.

The values of apparent degradation rate constants (k) of TC with initial concentration of 25 in presence of varying amount of CP/Ag are calculated and collected in Table 5. For real life applications the optimum amount of catalyst has to be determined in order to avoid excess catalyst and to ensure a total absorption of efficient photons [50].

The degradation result and membrane flux decline behavior (Table 6) obviously revealed that 0.8 g/L was the optimum CP/Ag loading.

The membrane flux decline behavior (Fig. 12) that clearly revealed in the range of 0.2–1 g/L was the optimum CP/Ag and CP loading. With regard to Fig. 12, it is seen that by increasing the amount of photocatalyst to 0.6 g/L, the amount of flux increases, but by increasing the amount of photocatalyst to 1 g/L, the amount of flux decreases that is due to the fouling of the membrane surface. Also, the amount of photocatalytic CP from CP/Ag is higher at all concentrations due to the absence of silver particles in its structure, which makes it easier to pass and has less membrane fouling.

The photocatalytic efficiency which has been improved regarding the TC fouling was approved by comparing the elimination of TOC in the photocatalytic membrane reactor as shown in Fig. 13. By applying only the UF membrane, the elimination of TOC was approximately 25% when there is no photocatalyst. Nevertheless, approximately 95% of elimination of the TOC was gained as the visible irradiation was combined with photocatalytic CP/Ag.

3.8. Effect of irradiation time

Generally, the kinetic behavior of photocatalytic reaction can be described by Langmuir–Hinshelwood equation confirming the heterogeneous catalytic character of the system. In this system, the rate r varying proportionally with the coverage θ as:

$$r = -\frac{dc}{dt} = k\theta = k\left(\frac{KC}{1+KC}\right)$$

where r is the rate of reaction in (mg/L min), k the rate constant for photocatalysis in (mg/L min), K the rate constant for adsorption in (L/mg) (Langmuir constant related to the energy of adsorption), C the concentration of dye solution in (mg/L), c the concentration of dye solution at any time, and t the time in minutes. For concentrations > 5.0 mM, ($KC \gg 1$), the reaction rate levels off and becomes independent of C and this leads to zero-order kinetics ($r = k_o$, where k_o is the zero-order rate constant). This is due to the occupying all of the catalytic sites on the catalyst surface by adsorbed reactant molecules at high concentration. For diluted solutions <1.0 mM, KC is $\ll1$ and the reaction rate
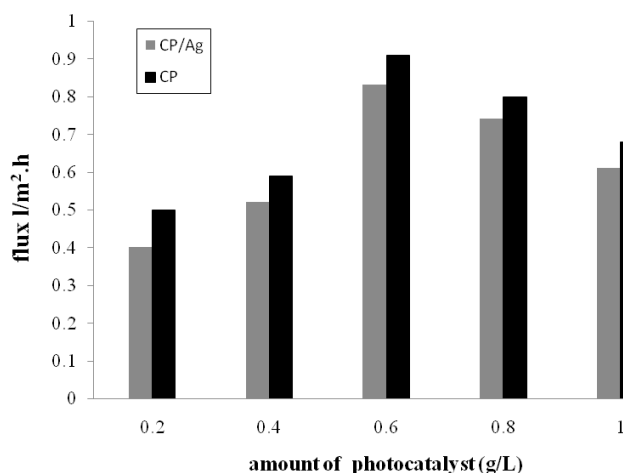
Fig. 12. Flux decline during the constant pressure ultrafiltration of 25 mg/L and pH 8 of TC solutions at 3 bars, in the presence of CP and CP/Ag with various photocatalyst loading.

Table 5
Degradation rate constant values (k) of TC as a function of various parameters. pH, 8; Initial conc. 25 (ppm), irradiation time, 2 h at 26°C

Amount of catalyst (g/L)	Value $k \times 100$ (min^{-1})
0.2	2.3
0.4	4.7
0.6	6.2
0.8	7.6
1	10.7

Table 6
Percentage of TC removal after photodegradation and UF filtration in PMR with various photocatalyst loading. pH, 8; Initial conc. 25 (ppm), irradiation time, 2 h at 26°C

CP/Ag loading (g/L)	TC degraded after Photocatalysis (%)	TC removal after UF Filtration (%)
0.2	43 ±1	99±0.5
0.4	78±1	99±0.5
0.6	92±1	99±0.5
0.8	95±1	99±0.5
1	96±1	99±0.5
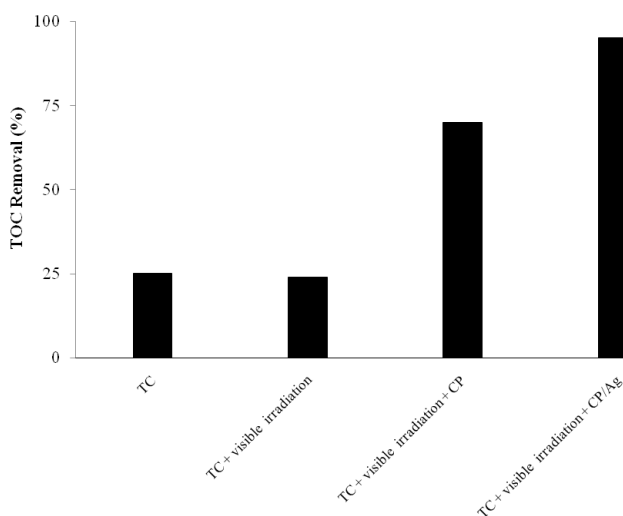
Fig. 13. TOC removal in photocatalytic membrane reactor: photocatalyst dosage, 0.5 g/l; pH, 8; initial concentration, 25 mg/L; irradiation time, 2 h at 26°C.

Table 7
Effect of irradiation time in TC degradation photocatalyst dosage, 0.5 g/l; pH, 8; at 26°C

Type of photocatalyst	Irradiation time (min)	Initial conc. (ppm)	Degradation efficiency (%)
CP/Ag	30	25	37
	60	25	63
	90	25	84
	120	25	92
CP	30	25	3
	60	25	13
	90	25	19
	120	25	24

Fig. 14. The effect of TC initial concentration on degradation efficiency of TC: pH, 8; photocatalyst concentration, 0.5 g/L; irradiation time, 2 h at 26°C.

is proportional to the initial concentration and the reaction is of the apparent first order ($r = -dc/dt = kKC = k_1C$ or $\ln C_t/C_o = -k_1 t$, where k_1 is a first-order rate constant in (min⁻¹)). At low concentrations, the number of catalytic sites will not be a limiting factor and the rate of degradation is proportional to the concentration of the TC [50–52].

As illustrated in Table 7, time is a major factor that impacts the efficiency of the degradation straightly. The experimental runs measuring the effect of irradiation time of 50 mL of TC solution with an initial concentration of 25 ppm in distilled water was treated with 500 mg of CP/Ag nanophotocatalyst and 500 mg of CP with irradiation time increment from 30 min to 120 min and is shown in Table 7. The outcome showed that degradation of TC is quick and only after 120 min of irradiation; the condition of equilibrium was reached. The apparent degradation rate constants (k values) as a function of the TC concentration are also calculated and collected in Table 5.

3.9. Effect of TC initial concentration

In order to utilize the photocatalytic oxidation in an efficient way, some research should be done to show that the rate of degradation actually is related and gets affected by the concentration of the substrate. The change in the inlet concentrations of the contaminant causes the rates of the reaction to change. According to Fig. 14, at the time that the initial TC's concentration becomes greater, the efficiency of the degradation reduces and this behavior has some causes. The quantity of the TC particles that are attracted to the active surface of the photocatalyst goes high at the time that the initial concentration of the pollutant goes high. In this situation, the pH, the catalyst dosage and the time of the reaction are maintained at the same value thus the quantity of the reactive species ($^\bullet OH$ and $^\bullet O_2^-$) does not change. As a result the current reactive radicals are not sufficient for the concentrations of TC that are high. Moreover, at the time that the concentration of the substrate reduces, the intermediates' production can happen and lead to diffuse in the surface of the photocatalyst which leads to deactivation of the reaction sites [53–55]. Therefore, the results show that by the increase in the initial concentration of the TC, the amount of catalyst surface that is sufficient for the degradation goes higher. It is possible that this is because of
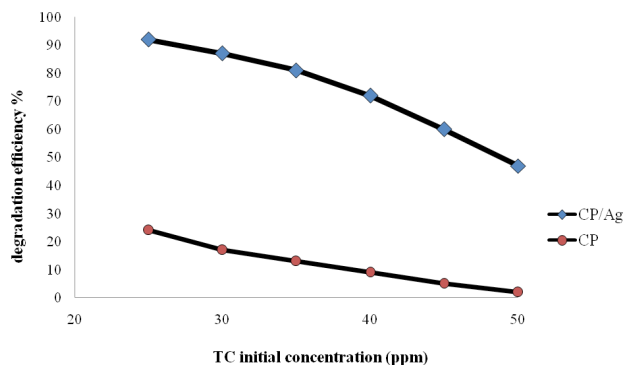
the shifting in the regime. The initial situation of the change is the condition in low concentrations that there is kinetic control regime. Then the system changes to some limitations at high concentrations. When photocatalytic oxidation happens, the concentration of organic substrate gets affected by the photonic efficiency. When the concentrations of the substrate are increased, there is a decrease in the photonic efficiency. Also the surface of the photocatalyst is filled and this results in the deactivation of the catalyst [56]. Moreover, if the concentration of the substrate gets high, this causes the intermediate materials to produce. Then those materials can be able to be absorbed on the catalyst's surface. This diffusion of the intermediate materials which has a slow rate can gradually cause the active sites to deactivate. This causes the rate of the degradation to decrease. When the concentrations are increases, the increasing concentrations of intermediate materials cause the radicals of hydroxyl to act as the limiting reactant which leads to the decrease in the degradation rate constants. As mentioned in the literature [57,58] $^\bullet OH$ can be formed by the reaction between hydroxide ion and positive hole. An alkaline condition would thus favor $^\bullet OH$ formation and enhance degradation efficiency [59–61]. Authors suggest that at high concentration of $-OH$, two processes may take place leading to the deactivation of $^\bullet OH$. First, the $H_2O_2^\bullet$ and $HO_2^\bullet$ radicals may be formed due to the reaction of $^\bullet OH$ with $-OH$. The reactivity of these radicals with organic dye is very low compared to that of $^\bullet OH$ [67]. Second, due to the presence of high amounts of $^\bullet OH$ radicals, the radical–radical reactions take place at higher pH values. This reaction was reported in the literature [61]. Generally, the deactivation of $^\bullet OH$ in high pH values was previously reported [58].

3.10. The effect of transmembrane pressure on permeate flux in the PMR

Fig. 15 shows the fact that the pressure of the transmembrane has effect on the permeate flux that is quantified for both UF membranes at the time of the PMR operation. In spite of applying the lowest cross flow velocity from all the examined values, TMP going up at the time of the experiments in the PMR caused the permeate flux to increase linearly in both UF membranes [22]. The fluxes measured during the experiments with CP slightly higher from CP/Ag was for all of the pressures that were examined. As it
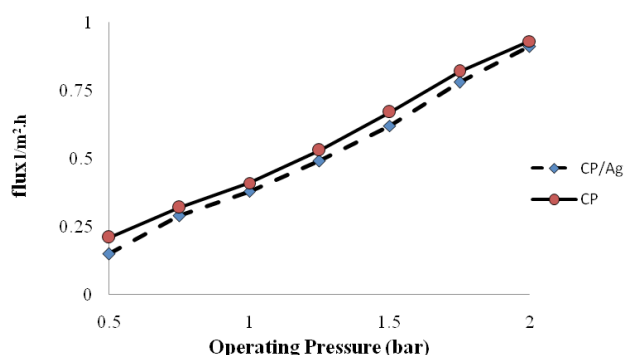
Fig. 15. The effect of operating pressure on the permeate flux.

is said before, the abrasion of the membranes' skin layer describes the detected increase in the flux.

4. Conclusions

In this research, zeolite clinoptilolite and its nanocomposite clinoptilolite zeolite-silver were synthesized by microwave irradiation prosperously and utilized as photocatalyst for the degradation of TC from synthesis wastewater. Diffuse reflectance spectroscopy illustrated an obvious trend of reduction in the band gap to the value of 2.47 eV when AgO was supported on CP. The specific surface area for the composited material reached 167 m^2/g, which was eight times larger than the unmodified AgO. Degradation of TC by using CP/Ag nanophotocatalyst was found to be a strongly pH dependent process. The increase in the concentration of the catalyst enhanced the efficiency of the degradation. This behavior is caused by the fact that the surface area or activated sites has increased. That outcome showed that degradation of TC is a quick process and only after 120 min of irradiation, the condition of equilibrium was also, results showed that optimum conditions for tetracycline degradation were found to be at pH of 9, photocatalyst dosage of 0.8 g/L and irradiation time of 120 min.

References

[1] R. Daghrir, P. Drogui, Tetracycline antibiotics in the environment: a review, Environ. Chem. Lett., 11 (2013) 209–227.

[2] T. An, J. An, H. Yang, G. Li, H. Feng, X. Nie, Photocatalytic degradation kinetics and mechanism of antivirus drug-lamivudine in TiO_2 dispersion, J. Hazard. Mater., 197 (2011) 229–236.

[3] M. Jiang, L. Wang, R. Ji, Biotic and abiotic degradation of four cephalosporin antibiotics in a lake surface water and sediment, Chemosphere, 80 (2010) 1399–1405.

[4] N. Arabpour, A. Nezamzadeh-Ejhieh, Modification of clinoptilolite nano-particles with iron oxide: increased composite catalytic activity for photodegradation of cotrimaxazole in aqueous suspension, Mater. Sci. Semicond. Process., 31 (2015) 684–692.

[5] N. Ajoudanian, A. Nezamzadeh-Ejhieh, Enhanced photocatalytic activity of nickel oxide supported on clinoptilolite nanoparticles for the photodegradation of aqueous cephalexin, Mater. Sci. Semicond. Process., 36 (2015) 162–169.

[6] J. Jeong, W. Song, W.J. Cooper, J. Jung, J. Greaves, Degradation of tetracycline antibiotics: Mechanisms and kinetic studies for advanced oxidation/reduction processes, Chemosphere, 78 (2010) 533–540.

[7] Y.J. Wang, D.A. Jia, R.J. Sun, H.W. Zhu, D.M. Zhou, Adsorption and cosorption of tetracycline and copper(II) on montmorillonite as affected by solution pH, Environ. Sci. Technol., 42 (2008) 3254–3259.

[8] F. Saadati, N. Keramati, M.M. Ghazi, Influence of parameters on the photocatalytic degradation of tetracycline in wastewater: A review, Crit. Rev. Environ. Sci. Technol., 46(8) (2016) 757–782.

[9] F. Yuan, C. Hu, X. Hu, D. Wei, Y. Chen, J. Qu, Photodegradation and toxicity changes of antibiotics in UV and UV/H_2O_2 process, J. Hazard. Mater., 185(2) (2011) 1256–1263.

[10] H. Liu, Y. Yang, J. Kang, M. Fan, J. Qu, Removal of tetracycline from water by Fe-Mn binary oxide, J. Environ. Sci., 24(2) (2012) 242–247.

[11] H. Derikvandi, A. Nezamzadeh-Ejhieh, Designing of experiments for evaluating the interactions of influencing factors on the photocatalytic activity of NiS and SnS2: Focus on coupling, supporting and nanoparticles, J. Colloid Interface Sci., 490 (2017) 628–641.

[12] A. Nezamzadeh-Ejhieh, Z. Salimi, Heterogeneous photodegradation catalysis of o-phenylenediamine using CuO/X zeolite, Appl. Catal. A., 390 (2010) 110–118.

[13] P. Mohammadyari, A. Nezamzadeh-Ejhieh, Supporting of mixed ZnS–NiS semiconductors onto clinoptilolite nano-particles to improve its activity in photodegradation of 2-nitrotoluene, Rsc Adv., 5(92) (2015) 75300–75310.

[14] A. Nezamzadeh-Ejhieh, A. Shirzadi, Enhancement of the photocatalytic activity of ferrous oxide by doping onto the nano-clinoptilolite particles towards photodegradation of tetracycline, Chemosphere, 107 (2014) 136–144.

[15] W.J. Liu, F.X. Zeng, H. Jiang, X.S. Zhang, W.W. Li, Composite Fe_2O_3 and ZrO_2/Al_2O_3 photocatalyst: preparation, characterization, and studies on the photocatalytic activity and chemical stability, Chem. Eng. J., 180 (2012) 9–18.

[16] M. Faisal, A.A. Ismail, A.A. Ibrahim, H. Bouzid, S.A. Al-Sayari, Highly efficient photocatalyst based on Ce doped ZnO nanorods: controllable synthesis and enhanced photocatalytic activity, Chem. Eng. J., 229 (2013) 225–233.

[17] S. Azimi, A. Nezamzadeh-Ejhieh, Enhanced activity of clinoptilolite-supported hybridized PbS–CdS semiconductors for the photocatalytic degradation of a mixture of tetracycline and cephalexin aqueous solution, J. Molec. Catal. A Chem., 408 (2015) 152–160.

[18] N.H.H. Hairom, A.W. Mohammad, A.A.H. Kadhum, Influence of zinc oxide nanoparticles in the nanofiltration of hazardous Congo red dyes, Chem. Eng. J., 260 (2015) 907–915.

[19] A. Moslehyani, A.F. Ismail, M.H.D. Othman, T. Matsuura, Hydrocarbon degradation and separation of bilge water via a novel TiO_2-HNTs/PVDF-based photocatalytic membrane reactor (PMR), RSC Adv., 5(19) (2015) 14147–14155.

[20] S. Mozia, K. Szymanski, B. Michalkiewicz, B. Tryba, M. Toyoda, A.W. Morawski, Effect of process parameters on fouling and stability of MF/UF TiO_2 membranes in a photocatalytic membrane reactor, Sep. Purif. Technol., 142 (2015) 137–148.

[21] C.S. Ong, W.J. Lau, P.S. Goh, B.C. Ng, A.F. Ismail, Investigation of submerged membrane photocatalytic reactor (sMPR) operating parameters during oily wastewater treatment process, Desalination, 353 (2014) 48–56.

[22] S. Mozia, D. Darowna, A. Orecki, R. Wrobel, K. Wilpiszewska, A.W. Morawski, Microscopic studies on TiO_2 fouling of MF/UF polyethersulfone membranes in a photocatalytic membrane reactor, J. Membr. Sci., 470 (2014) 356–368.

[23] V. Augugliaro, M. Litter, L. Palmisano, J. Soria, The combination of heterogeneous photocatalysis with chemical and physical operations: A tool for improving the photoprocess performance, J. Photochem. Photobiology., 7(4) (2006) 127–144.

[24] P. Jeffrey, B. Jefferson, Public receptivity regarding "in-house" water recycling: results from a UK survey, Water Sci. Technol. Water Supply, 3(3) (2003) 109–116.

[25] M.H. Sheikh-Mohseni, A. Nezamzadeh-Ejhieh, Modification of carbon paste electrode with Ni-clinoptilolite nanoparticles for electrocatalytic oxidation of methanol, Electrochim. Acta., 147 (2014) 572–581.

[26] J. Esmaili-Hafshejani, A. Nezamzadeh-Ejhieh, Increased photocatalytic activity of Zn(II)/Cu(II) oxides and sulfides by coupling and supporting them onto clinoptilolite nanoparticles in the degradation of benzophenone aqueous solution, J. Hazard. Mater., 316 (2016) 194–203.

[27] A. Nezamzadeh-Ejhieh, Z. Ghanbari-Mobarakeh, Heterogeneous photodegradation of 2, 4-dichlorophenol using FeO doped onto nano-particles of zeolite P, J. Ind. Eng. Chem., 21, (2015) 668–676.

[28] A. Bagheri Ghomi, V. Ashayeri, Photocatalytic efficiency of $CuFe_2O_4$ by supporting on clinoptilolite in the decolorization of acid red 206 aqueous solutions, Iranian J. Catalysis, 2(3) (2012) 35–140.

[29] A. Nezamzadeh-Ejhieh, S.Moeinirad, Heterogeneous photocatalytic degradation of furfural using NiS-clinoptilolite zeolite, Desalination, 273 (2011) 248–257.

[30] M.M.J. Treacy, J.B. Higgins, R.V. Ballmoos, Collection of Simulated XRD Powder Patterns for Zeolites, IZA Publications, 1996.

[31] M. Rivera-Garza, M.T. Olguin, I. Garcia-Sosa, D. Alcantare, G. Rodriguez-Fuentes, Silver supported on natural Mexican zeolite as an antibacterial material, Micropor. Mesopor. Mater., 39(3) (2000) 431–444.

[32] M. Bordbar, S. Forghani-pilerood, A. Yeganeh-Faal, Enhanced photocatalytic activity of sonochemical derived ZnO via the co-doping process, Iranian J. Catal., 6(5) (2016) 415–421.

[33] M. Bordbar, T. Alimohammadi, B. Khoshnevisan, B. Khodadadi, A. Yeganeh-Faal, Preparation of $MWCNT/TiO_2$–Co nanocomposite electrode by electrophoretic deposition and electrochemical study of hydrogen storage, Int. J. Hydrogen Energy, 40 (2015) 9613–9620.

[34] C. Orha, F. Manea, C. Ratiu, G. Burtica, A. Iovi, Obtaining and characterization of Romanian zeolite supporting silver ions, Environ. Eng. Manag. J., 6 (2007) 541–544.

[35] M.S.L. Yee, P.S. Khiew, Y.F. Tan, W.S. Chiu, Y.Y. Kok, C.O. Leong, Low temperature, rapid solution growth of antifouling silver-zeolite nanocomposite clusters, Microporous Mesoporous Mater., 218 (2015) 69–78.

[36] K.K. Krishnani, Y. Zhang, L. Xiong, Y. Yan, R. Boopathy, A. Mulchandani, Bactericidal and ammonia removal activity of silver ion-exchanged zeolite, Bioresour. Technol., 117 (2012) 86–91.

[37] A. Nezamzadeh-Ejhieh, S. Khorsandi, Photocatalytic degradation of 4-nitrophenol with ZnO supported nano-clinoptilolite zeolite, J. Ind. Eng. Chem., 20(3) (2014) 937–946.

[38] H.H. Cheng, C.C. Hsieh, C.H. Tsai, Antibacterial and regenerated characteristics of Ag-zeolite for removing bioaerosols in indoor environment, Aerosol. Air. Qual., 12 (2012) 409–419.

[39] S. Zhong, F. Zhang, B. Yu, P. Zhao, L. Jia, S. Zhang, Synthesis of $PVP-Bi_2WO_6$ photocatalyst and degradation of tetracycline hydrochloride under visible light, J. Mater. Sci: Mater. Electron., 27(3) (2016) 3011–3020.

[40] T.K. Ghorai, N. Biswas, Photodegradation of Rhodamine 6G in aqueous solution via $SrCrO_4$ and TiO_2 nano-sphere mixed oxides, J. Mater. Rese. Technol., 2 (2013) 10–17.

[41] M. Anpo, M. Takeuchi, The design and development of highly reactive titanium oxide photocatalysts operating under visible light irradiation, J. Catalysis, 216 (2003) 505–516.

[42] M.Addamo, V. Augugliaro, A. Di Paola, E. Garcia-Lopez, V. Loddo, G. Marci, L. Palmisano, Removal of drugs in aqueous systems by photoassisted degradation, J. Appl. Electrochem., 35(7–8) (2005) 765–774.

[43] J. Saien, A.R. Soleymani, Degradation and mineralization of Direct Blue 71 in a circulating upflow reactor by UV/TiO_2 process and employing a new method in kinetic study, J. Hazard. Mater., 144 (2007) 506–512.

[44] N. Keramati, B. Nasernejad, N. Fallah, Synthesis of $N-TiO_2$: Stability and visible light activity or aqueous styrene degradation, J. Dispersion Sci. Tech., 35(10) (2014) 1476–1482.

[45] S. Jafari, A. Nezamzadeh-Ejhieh, Supporting of coupled silver halides onto clinoptilolite nanoparticles as simple method for increasing their photocatalytic activity in heterogeneous photodegradation of mixture of 4-methoxy aniline and 4-chloro-3-nitro aniline, J. Colloid Interface Sci., 490 (2017) 478–487.

[46] S. Mousavi-Mortazavi, A. Nezamzadeh-Ejhieh, Supported iron oxide onto an Iranian clinoptilolite as a heterogeneous catalyst for photodegradation of furfural in a wastewater sample, Desal. Water Treat., 57(23) (2016) 10802–10814.

[47] Z.A. Mirian, A. Nezamzadeh-Ejhieh, Removal of phenol content of an industrial wastewater via a heterogeneous photodegradation process using supported FeO onto nanoparticles of Iranian clinoptilolite, Desal. Water Treat., 57(35) (2016) 16483–16494.

[48] V. Buscio, M.J. Marín, M. Crespi, C. Gutiérrez-Bouzán, Reuse of textile wastewater after homogenization–decantation treatment coupled to PVDF ultrafiltration membranes, Chem. Eng. J., 265 (2015) 122–128.

[49] Y. Nakaoka, H. Katsumata, S. Kaneco, T. Suzuki, K. Ohta, Photocatalytic degradation of diazinon in aqueous solution by platinized TiO_2, Desal. Water Treat., 13 (2010) 427–436.

[50] A. Nezamzadeh-Ejhieh, S. Hushmandrad, Solar photodecolorization of methylene blue by CuO/X zeolite as a heterogeneous catalyst, Appl. Catal. A., 388 (2010) 149–159.

[51] J.M. Herrmann, Heterogeneous photocatalysis: fundamentals and applications to the removal of various types of aqueous pollutants, Catal. Today., 53 (1999) 115–129.

[52] S. Parra, S.E. Stanca, E. Guasaquillo, K.R. Thampi, Photocatalytic degradation of atrazine using suspended and supported TiO_2, Appl. Catal. B: Environ., 51 (2004) 107–116.

[53] N. Daneshvar, S. Aber, M.S. SeyedDorraji, A.R. Khataee, M.H. Rasoulifard, Sorption of divalent metal ions from aqueous solution by carbon nanotubes: a review, Sep. Purif. Process., 58 (2007) 91–98.

[54] U.I. Gaya, A.H. Abdullah, Heterogeneous photocatalytic degradation of organic contaminants over titanium dioxide: a review of fundamentals, progress and problems, J. Photochem. Photobiology C: Photochem. Rev., 9 (2008) 1–12.

[55] V.A. Sakkasa, P. Calzab, A.D. Vlachoua, C. Medanab, C. Minerob T. Albanis, Appl. Catal. B: Environ., 110 (2011) 238–250.

[56] J. Aran, J.L.M. Nieto, J.A.H. Melian, J.M.D. Rodriguez, O.G. Diaz, J.P. Perna, C.A. Bergasa, J. Mendez, Photocatalytic degradation of formaldehyde containing wastewater from veterinarian laboratories, Chemosphere, 55(6) (2004) 893–904.

[57] A. Nezamzadeh-Ejhieh, M. Khorsandi, Heterogeneous photodecolorization of Eriochrome Black T using Ni/P zeolite catalyst, Desalination, 262(1–3) (2010) 79–85.

[58] M.B. Kasiri, H. Aleboyeh, A. Aleboyeh, Degradation of Acid Blue 74 using Fe-ZSM5 zeolite as a heterogeneous photo-Fenton catalyst, Appl. Catal. B: Environ., 84 (2008) 9–15.

[59] H.R. Pouretedal, A. Norozi, M.H. Keshavarz, A. Semnani, Nanoparticles of zinc sulfide doped with manganese, nickel and copper as nanophotocatalyst in the degradation of organic dyes, J. Hazard. Mater., 162 (2009) 674–681.

[60] J. Saien, A.R. Soleymani, Degradation and mineralization of Direct Blue 71 in a circulating up flow reactor by UV/TiO_2 process and employing a new method in kinetic study, J. Hazard. Mater., 144 (2007) 506–512.

[61] S. Ashraf, M.A. Rauf, S. Alhadrami, Degradation of Methyl Red using Fenton's reagent and the effect of various salts, Dyes. Pigm., 69 (2006) 74–78.